DEFENCE
SCIENCE & TECHNOLOGY

Principal Component Thermography

N. Rajic

DSTO-TR-1298

20020919 065

Principal Component Thermography

N. Rajic

Airframes And Engines Division
Aeronautical and Maritime Research Laboratory

DSTO-TR-1298

ABSTRACT

This report describes a robust computational framework for the qualitative enhancement and quantitative interpretation of active thermographic inspection data. Singular Value Decomposition is used to reduce an appropriately constructed matrix of raw pixel values to a set of orthogonal functions that compactly describe the key spatial and temporal variations relating to underlying structural anomalies. Tests against synthetic and experimental data are described that underscore the practical efficacy of the methodology, and demonstrate significant advantages compared to more traditional methods of processing.

APPROVED FOR PUBLIC RELEASE

AO FO2-12-3327

APPROVED FOR PUBLIC RELEASE

Principal Component Thermography

EXECUTIVE SUMMARY

Active thermal inspection technology, recently introduced into the RAAF, promises to provide a lower cost alternative to current nondestructive inspection methodologies for a wide range of structural integrity problems in F/A-18 and F-111 aircraft. The capacity of pulse thermography to furnish highly-informative broad-field inspection data for large structural components in a remarkably short time holds great practical appeal, and has served to accelerate its uptake amongst military and civilian fleet owners around the world. The technology is however deficient in (i) having a limited penetration depth compared to alternative active NDT (nondestructive testing) methods, and (ii) the considerable difficulty involved in obtaining robust and precise measures for various defect characteristics. These issues continue to stimulate vigorous research activity. Although a number of useful advancements have been made on these matters, much scope for improvement and further development remains.

The present study reports on a new methodology that provides an integrated framework for both contrast enhancement and flaw depth estimation based on the singular value decomposition of an appropriately constructed matrix of observations. The methodology is shown to produce a highly compact and useful representation of the spatial and temporal variations relating to contrast information associated with underlying structural flaws. The method does not rely on the explicit formation of a contrast response, required by traditional approaches, and accordingly avoids the consequent risk of introducing bias in the flaw depth prediction. Synthetic and experimental data sets are analysed to underscore the practical efficacy of the methodology, its robustness to noise and bias, and a superior level of performance compared to pulse phase thermography.

Author
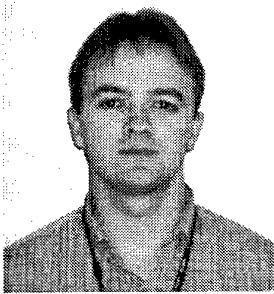
Nik Rajic
Airframes and Engines Division

Nik Rajic received a B. Eng. (Hons.) in Mechanical Engineering from the University of Melbourne in 1989. He joined Structures Division at the Aeronautical Research Laboratory in 1991 and in 1992 undertook studies at Monash University which led to the completion of a PhD in 1995. He has since contributed to research on fatigue-life extension techniques, thermoelastic stress analysis, thermoplasticity, thermographic nondestructive evaluation, and in situ structural health monitoring techniques based on smart structures principles. He is currently a Senior Research Scientist in the Airframes and Engines Division.

Contents

Figures

1 Introduction

Active infrared thermography is a broad-field non-contact non-destructive inspection technique with immense practical appeal. However, it has at least two notable deficiencies: (i) a limited penetration depth compared to other active inspection techniques like ultrasound and radiography, and (ii) only a modest quantitative capability; a consequence of the profound difficulty involved in deriving robust measures for flaw depth and other defect characteristics based on thermal inspection data. Although significant progress has been made on these matters over the past decade, they still warrant, and continue to attract, considerable research activity.

Improvements in penetration depth for example, have occurred naturally as a consequence of better signal-to-noise ratios achieved through the evolution of infrared detection technology, but also directly through the development of processing techniques that are able to furnish flaw contrasts substantially higher than that typically available from raw data. These include box-car and synchronous averaging (see Rajic (2001) for example), least squares background minimisation (Plotnikov et al (2000)), time derivative computation (Cramer et al (1995)), pulsed phase thermography (Maldague & Marinetti (1996)), and computational pulse shaping (Winfree (1998)).

Substantial progress has also been made in developing a useful quantitative capability, with notable advancements in thermal diffusivity estimation (see Winfree & Heath (1998)) and flaw depth characterisation. With regard to the latter, most of the techniques that have been reported function by exploiting correlations between the observed temperature-time evolution and that predicted analytically, normally for an idealised representation of the heat conduction problem involving a semi-infinite slab and one-dimensional heat flow. For example, Ringermacher et al (1998) develop an expression using one-dimensional heat flow theory that relates the flaw depth to the delay between the excitation event and the development of an inflection in the contrast evolution. Alternatively, the entire early phase of the contrast response history can be encompassed in an optimisation process (Rajic (2001)) where the object is to minimise the residual error between the observations and predictions based on one-dimensional heat flow in a slab of finite thickness. Data redundancy leads to good robustness to experimental noise and, since it accommodates finite slab-thickness, the method should yield better estimates than the inflection-time approach when the flaw depth is small, albeit with increased computational expense.

A valid criticism of methods, like these, that rely on the formation of a contrast evolution is that biases may be introduced if the reference point is not carefully selected. Measures like employing an averaged reference, formed over a number of carefully chosen pixels, can be effective in reducing the scope for bias. Alternatively, a suitable reference can be synthesized. From a practical viewpoint, it is vital that such approaches are applied transparently in order to preserve simplicity and generality.

An alternative methodology, reported in Shepard et al (2001), focuses on the deviation in the observed raw response from ideal transient behaviour defined by the impulse response of a semi-infinite slab. This divergence occurs at a time close to the inflection point in an equivalent contrast response curve. The computation is performed on a synthetic response modelled on the raw data using a set of non-orthogonal logarithmic basis functions, which facilitates a more noise-tolerant basis for detecting departure from ideal

behaviour.

The present study reports on the application of empirical orthogonal function analysis to the decomposition of active thermographic inspection data. This approach provides an integrated framework for both contrast enhancement and flaw depth estimation based on a single computation applied to an appropriately constructed data matrix. Singular value decomposition (SVD) is used to reduce the matrix of observations to a highly compact statistical representation of the spatial and temporal variations relating to contrast information associated with underlying structural flaws. These variations are described in modes or basis functions that are orthogonal and inherently characteristic of the experimental data, features that are seldom found in more conventional analytically-based decomposition methodologies. Additionally, no reliance is placed on the explicit formation of a contrast response. Interestingly, the computation does however yield a characteristic time function that is shown to be related to the contrast evolution and can be used as a basis for flaw depth characterisation. After outlining the salient computational details of the methodology, synthetic and experimental data sets are analysed to underscore its practical efficacy and to demonstrate its robustness to noise and bias.

2   Computational Details

Empirical orthogonal function (EOF) analysis (Emery and Thomson (1998)) provides a framework for constructing a set of orthogonal statistical modes that furnish a complete description of the variability in a set of observations. The analysis involves the calculation of a covariance matrix or, alternatively, the application of a singular value decomposition. The latter is computationally more efficient and is the approach employed in the present work. When applied to thermographic data, this analysis produces a remarkably compact description of the salient spatial and temporal signal variations relating to the contrasts associated with underlying structural flaws. In many cases, a richly informative description of these contrasts is furnished in a single spatial mode and its complimentary characteristic time vector, known as the principal component.

Data acquired in the course of a normal active thermal inspection is customarily organised in the manner depicted in *Figure 1*, a three dimensional array, which, for convenience, is defined here as $T(i, j, k)$, where $i = 1, 2, \ldots, N_x$, $j = 1, 2, \ldots, N_y$, and $k = 1, 2, \ldots, N_t$. The pixel values in each image frame are drawn out into a vector to condense the original data "cube" into a matrix A with dimension $M \times N$, where $M = N_x * N_y$ and $N = N_t$. Each of the M column vectors are then subjected to a standardisation process to ensure uniform variance on a pixel by pixel basis, viz.,

$$\hat{A}(n, m) = \frac{A(n, m) - \mu_m}{\sigma_m} \tag{1}$$

where
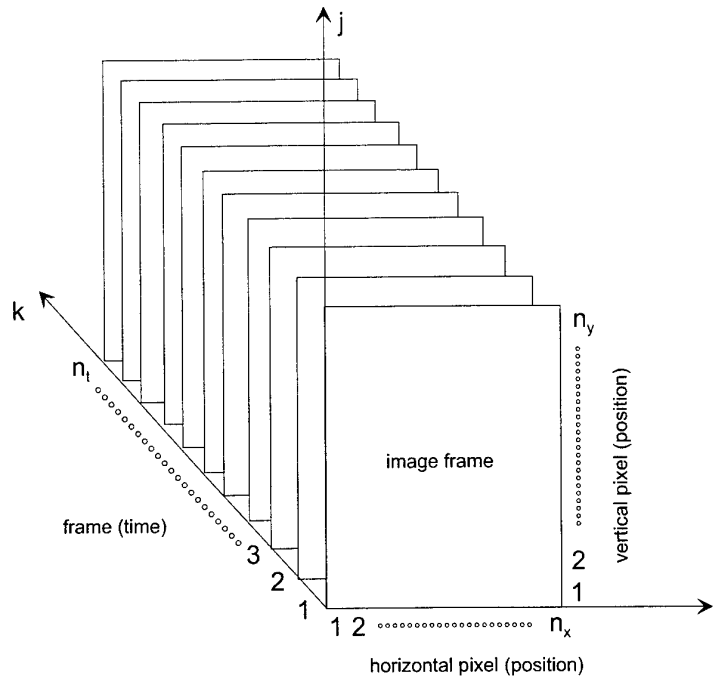
$$\mu_m = \frac{1}{N} \sum_{n=1}^{N} A(n, m) \tag{2}$$

Figure 1: Sequence of n_t image frames each with $n_x \times n_y$ elements.

and

$$\sigma_m^2 = \frac{1}{N-1} \sum_{n=1}^{N} (A(n,m) - \mu_n)^2 \tag{3}$$

This standardised matrix $\hat{A}$ is then reduced by singular value decomposition as follows,

$$A = U * \Gamma * V^T \tag{4}$$

where, if $M > N$, Γ is an $N \times N$ diagonal matrix with positive or zero elements representing the singular values of matrix A, U is an $M \times N$ matrix, and V^T is the transpose of an $N \times N$ matrix. Given the structure described for the data matrix A, the columns of matrix U contain the orthogonal modes describing the spatial variations in the observations. The contributions of the modes to the response are proportional to the corresponding singular values, and vary in time according to the coefficients in the associated principal components, or eigenfunctions, which appear row-wise in matrix V^T.

The spatial modes contained in U are reformed into a two-dimensional array by reversing the condensation of the raw data matrix T, described earlier. The corresponding principal components are one-dimensional vectors and require no modification.

The analysis yields a total of N_t spatial and temporal modes, which together comprise a complete description of the information contained in the original data cube. It is evident from the array sizes that storage requirements are greater for the products of

the decomposition than for the original form, which belies the supposed compactness of the representation. Its efficiency, in fact, stems from the reorganisation of information according to spatial scale, which allows for the elimination of a high proportion of modes corresponding to finer spatial scales where, invariably, the dominant signal feature is noise. This is especially appropriate in the thermal inspection context, since the underlying physical process: heat conduction, selectively attenuates features with high spatial frequency, much like a low-pass filter. Normally, modes corresponding to all but the largest scales can be discarded with little loss of information. Indeed, in the present work, analyses on uncontaminated synthetic data have shown that the first two modes typically account for more than 99% of the total data variance. This amounts to a very useful reduction in storage burden, and, incidentally, suggests a promising strategy for the compression of thermographic data sequences.

Of the signal variance explained by the first two modes, only a small proportion relates to thermal contrast information. Significantly, this information tends to condense into a single mode, furnishing a useful level of contrast enhancement. The advantages of a condensed representation are clear. From a practical standpoint, an operator is able to collapse a transient record made up of many frames into a single image containing the salient contrast information, and is consequently better positioned to make a rapid assessment of structural integrity. Also, it fosters a strong correlation between the principal component and the contrast evolution, which, in turn, provides a basis for the characterisation of flaw depth. Finally, it enables further gains in storage efficiency. In principal, a sequence of N_t frames could be replaced by a single image reducing the storage requirement by a factor $\frac{1}{N_t}$.

It is helpful to consider a thermal inspection sequence as comprising, approximately, two components, as illustrated in *Figure 2*: (i) a multi-modal spatially-uniform transient decay and (ii) a spatially non-uniform component representing the thermal contrasts. This provides a conceptual framework that assists in relating the modal and primordial representations. For instance, modal decompositions of active thermal inspection data typically produce a first mode characterised by a largely uniform spatial field with an exponential time decay, that accounts for the main portion of total observation variance. Its resemblance to the decaying field observed in practice is strikingly obvious. The second mode is weaker, accounting for a much lower proportion of total variance, but is strongly coherent with thermal contrasts associated with hidden structural anomalies and is consequently more useful in a nondestructive inspection context. It is useful to ascribe to the second EOF a contextual description, so hereon this function is referred to as the primary contrast mode (PCM).

The separation of an active thermal response into uniform and contrast components is only approximate. Whilst the projection of contrast information is strongest in the second mode, the statistical character of the decomposition allows for leakage into other modes. If however, the second mode accounts for the main shape of the contrast indication, successive modes, through orthogonality, must assume complex shapes which are unlikely to resemble the contrast spatial signature. Accordingly, these higher modes are less useful in a practical sense. Additionally, the finer spatial scales that these modes represent imply increasing exposure to noise, and a consequent likelihood of decreased robustness.

It is worth also noting the distinction between these statistical modes and the system
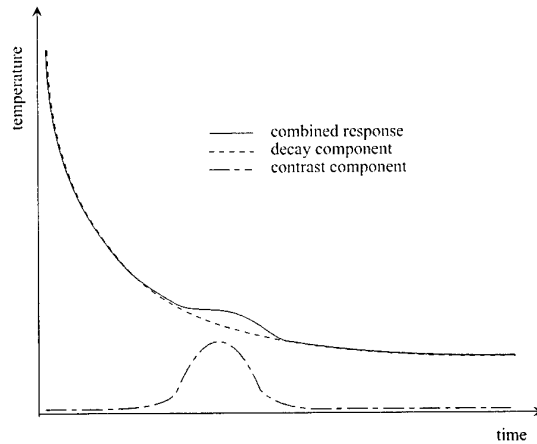
Figure 2: Conceptual separation of decay and contrast components of an active thermal inspection signal.

(or thermal) modes. The latter are characterised by exponential decay, whereas the orthogonal statistical modes have no such restriction. Further, it is speculated that a proper system modal-decomposition would not produce the level of contrast refinement observed for the primary contrast mode, based on an expectation that contrast information would be spread across many system modes. Such a comparison would be worthwhile, and will be pursued in a sequel to the present study.

3 Contrast Enhancement Performance

The functioning of the approach is best demonstrated by considering an appropriate example. Synthetic thermal response data was produced by running a simulation of transient axisymmetric heat-flow in an aluminium slab containing a circular blind hole. *Figure 3* shows a cross-sectional view of the structure. The relevant dimensions in this figure are a =64 mm and d =10 mm. A uniform heat flux of arbitrary strength Q was applied to the surface $z = 0$ and the response sampled at 64 evenly-spaced nodal positions (1 mm separation) over a 1 second duration at a time interval of 5 milliseconds. To better represent physical measurements, the data was contaminated with Gaussian noise affecting a signal-to-noise ratio (SNR) of 10, viz.,

$$\frac{\sigma_N}{C_{max}} = 0.1 \tag{5}$$

where σ_N is the standard deviation of the noise and C_{max} is the peak spatial contrast in the frame sequence, defined here as: $max|T_{r=0,j} - T_{r=a,j}|$, where j is the time index at which the maximum spatial contrast is observed. A useful indication of SNR is given in *Figure 4* which shows a surface plot of the response at peak contrast formed by applying an appropriate coordinate transformation to the two-dimensional data set. *Figure 5* shows a comparison amongst the peak contrast distribution and the first 4 EOF's. To better
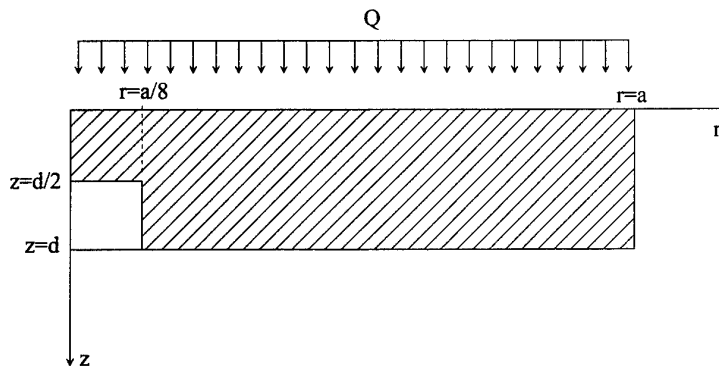
Figure 3: Test problem geometry.

illustrate the structure of each EOF, and to provide a baseline for the assessment of the noise-sensitivity of each mode, the analysis was also applied to the uncontaminated data.

The first mode shown in *Figure 5* corresponds to the largely homogeneous decay, which accounts for about 80% of the variability in the contaminated data sequence and 99% in the raw set. Although the mode appears to have a uniform shape, this is merely an artefact of the scaling furnished by the decomposition and preserved in *Figure 5*. Closer inspection reveals a slight deviation in the central region, adjacent to the structural flaw, amounting to a 0.08% relative change from the baseline. Although small, the deviation is clearly discernable at a modified scale, due to the relatively high signal to noise ratio.

The second mode accounts for about 0.6% of the variability in the contaminated data and about 0.7% in the raw data. It strongly accords with the peak contrast distribution (top curve), which signifies a close relationship with the underlying structural flaw. Also, the mode is seen to be relatively "clean", with a signal to noise ratio noticeably higher than that for the peak contrast distribution. This suggests a useful level of noise-rejection, which is an essential feature for practical application.

The higher modes shown in *Figure 5* differ markedly in shape to the physical contrast signal, whereby each successive mode contains an additional extremum. The essential reason for the increased complexity in shape was outlined earlier. In addition, these higher modes are evidently more prone to noise contamination, largely because they capture spatial variations on an increasingly finer scale. Referring again to *Figure 5*, it is evident that the shape of the fourth EOF is completely obscured by noise.

3.1 Sensitivity to Excitation Non-uniformities

The provision of a spatially uniform illumination is important in thermographic inspections because it improves the likelihood that spatially varying features in the thermal response data will relate to underlying structural features, and not to thermal artefacts produced by uneven heating. Unfortunately, in practice, a perfectly uniform illumination is seldom achievable. Accordingly, useful processing methodologies need to be able to cope with some degree of excitation non-uniformity.
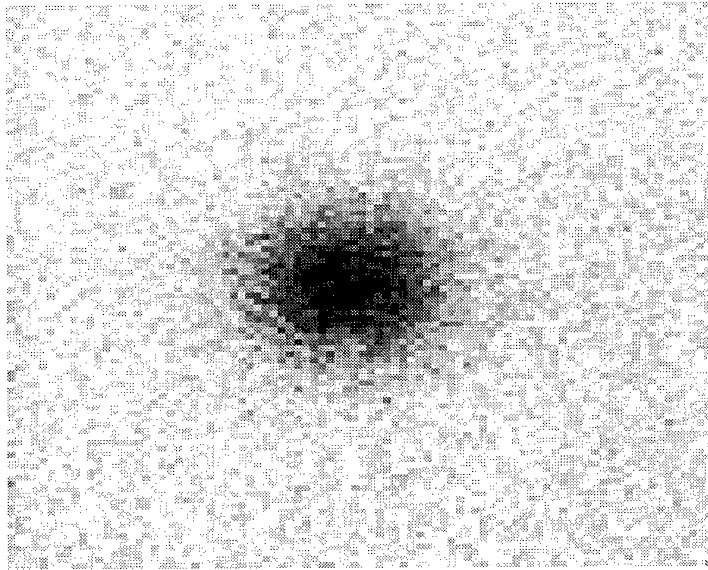
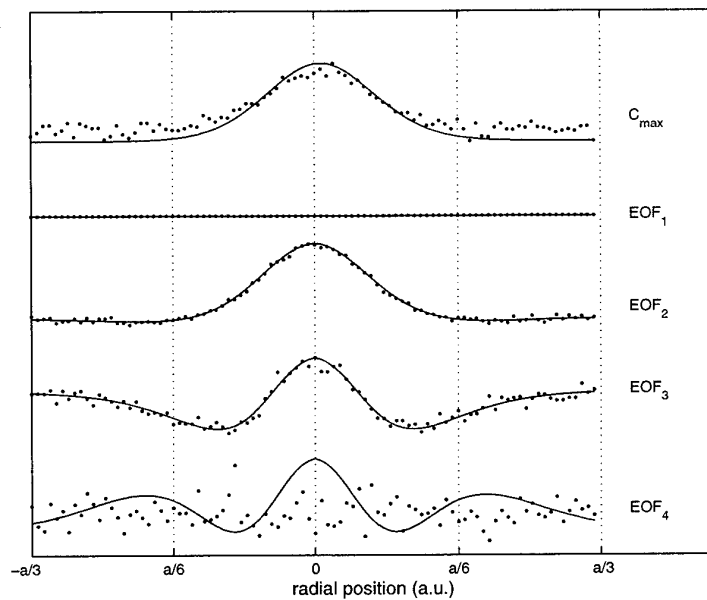*Figure 4: Response at peak contrast.*

Figure 5: Comparison amongst modes 1 to 4 and the peak contrast distribution for synthetically generated data with and without noise contamination.
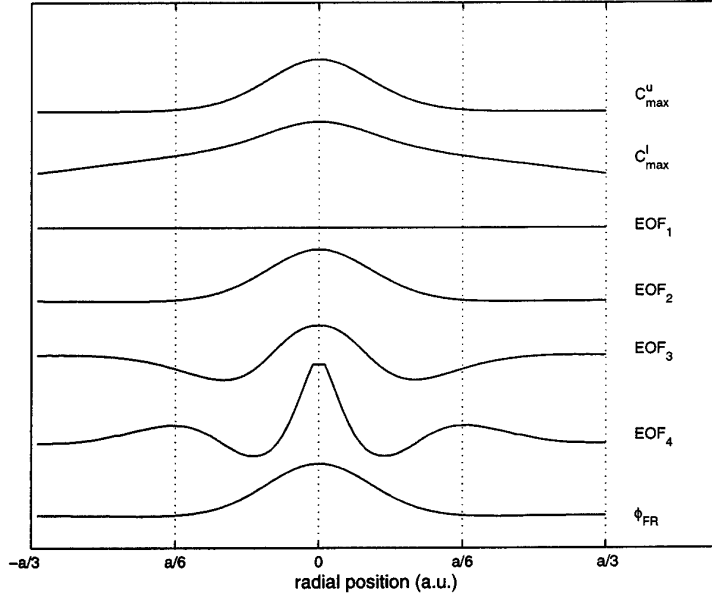
Figure 6: As for Figure 5, except for linear heat flux distribution. Superscripts u and l denote uniform and linear flux cases respectively, and ϕ_{FR} denotes the phase distribution at the frequency resolution.

A relatively new processing technique that is notably robust in this regard is pulse phase thermography (PPT) (Maldague (1996)). Its success stems from an intrinsic property whereby multiplicative signal components are completely rejected. This includes field variations induced by illumination non-uniformities, at least those with a spatial scale large compared to that of contrasts relating to underlying flaws. The origins of this useful property will be outlined in the next section. The immediate aim here is to undertake a comparison of the sensitivities of the second EOF and a phase map to spatial variations in illumination, using a slightly modified form of the data sequence produced in the earlier heat-flow simulation. The modification comprised a linear, instead of uniform, surface flux variation described by,

$$Q(r) = Q_o \mid 2 - \frac{r}{a} \mid \tag{6}$$

As anticipated, the primary effect of the uneven flux is to introduce a bias in the surface temperature profile, shown in the second curve in *Figure 6*. Interestingly, no evidence of any bias is present in the PCM (EOF_2), which has a shape similar to that of the original response (top curve), and to the phase distribution (bottom curve) at the frequency resolution, which, for the case at hand, is 1 Hz.

A reasonable question then is where within the modal representation does this type of information appear. Since the effect of the bias is characterised by a large spatial scale, it might be reasonable to expect a strong projection to the first mode. However, it is important to recall that the illumination field acts like a spatially varying gain factor, and does not significantly impact the time behaviour. Accordingly, it is not likely to

project into any single mode. Indeed, the first mode shape revealed no evidence of a linear trend. Moreover, there is little noticeable difference between the mode shapes presented in *Figure 6* and those obtained for a uniform heat flux (*Figure 5*), suggesting that the variance may be distributed across any number of higher modes.

3.2 Other Comparisons with Pulse Phase Thermography

In view of the growing use of pulse phase thermography by the thermographic community (Couturier & Maldague (1997), Marinetti *et al* (1999)), it is useful to consider further comparisons between PPT and PCT methods. First, a brief outline of the underlying principles of PPT is appropriate.

In essence, PPT employs a direct Fourier transform applied time-wise to each pixel to form a map of phase at a prescribed frequency. Specifically, the time history at each pixel location is transformed to a complex Fourier spectrum, viz.,

$$F_u = \frac{1}{N} \sum_{i=0}^{N-1} f_k \, e^{-\frac{2\pi i}{N} ku} \tag{7}$$

where the phase at each frequency u is given, essentially, by the ratio of the imaginary and real components of F_u, viz.,

$$\phi_u = \mathrm{atan}(\frac{Im \mid F_u \mid}{Re \mid F_u \mid}) \tag{8}$$

That multiplicative effects are rejected is immediately evident from *Eqn 8*. Note that a weakly non-uniform illumination, where the impetus for lateral heat flow is low, may be approximated by a uniform field modulated by a gain function describing the spatial variation. A Fourier decomposition would then comprise quadrature and in-phase components with identical gain factors describing the modulation, which cancel in the phase computation (*Eqn 8*). A physical interpretation is also helpful. Consider that a shallow illumination gradients tend to provide little impetus for lateral heat flow and consequently induce little variation in the time behaviour across pixels. Since phase is largely a measure of time delay, it follows that the variation in phase should be concomitantly small.

Similar reasoning can be applied to explain the rejection of surface emissivity variations. In practice, evident variations can often be reduced by coating the article with a uniformly thin layer of high emissivity paint. However, circumstances do arise where surface modification is disallowed, for instance, where a likelihood exists that paint may react with an existing surface coating. Inspections done under these sub-optimal conditions are likely to yield emissivity artefacts.

There is one evident distinction, in a post-processing context, between surface emissivity variations and illumination non-uniformities. Whilst the effects of illumination unevenness are characterised by a large spatial scale, those relating to emissivity can occur at arbitrary length scales. Accordingly, it might be expected that the performance of the PCT method with respect to rejecting emissivity variations would diminish as the length scale approaches that of any underlying flaw. Investigations so far indicate no

such sensitivity and suggest little difference in the performance of PCT and PPT methods. Generally, it is found that time-invariant elements of a signal, whether resembling a gain or offset, do not project into the significant modes of variance, nor, by definition, do they represent distinct modes of variance in themselves. In practice, both illumination non-uniformities and emissivity variations can be characterised as gain factors, and are consequently rejected in the PCM, although it must be stressed that severe illumination non-uniformities exciting substantial lateral heat flows are likely to affect a change in the PCM.

The performance of PPT and PCT methods at rejecting emissivity variations can be illustrated by example. To this end, the data sequence derived from the heat-conduction simulation described earlier was subject to slight modification. Specifically, pixel values within a rectangular region, encompassing part of the flaw, were modulated by a constant gain factor of 0.5. PPT and PCT analyses were then applied to the modified data sequence and a supplementary sequence contaminated by Gaussian distributed noise with variance set to achieve a SNR of 10. *Figure 7* shows that the impact of the emissivity artefact on the peak contrast thermograms (top row) is profound, serving to partially obscure the underlying flaw indication. In contrast, the pair of phase images in the second row show no evidence of the band whatsoever, which is anticipated since the Fourier transform projects all gain-related information in the amplitude map (3rd row). Importantly, the PCM or the 2nd EOF, is similar to the phase image in its lack of any discernable evidence of the artefact. Incidentally, the PCM for the contaminated data set has a noticeably higher signal to noise ratio compared to the equivalent phase image.

Unlike the example considered in §3.1, traces of the artefact were identifiable in the EOF's obtained for the case at hand. Remnants of the horizontal band were generally evident across a large number of higher order functions, but was most pronounced in the 6th EOF, which is shown in *Figure 7*. Modes beyond the 5th were found to contribute little to the signal variance, about 0.05%, which is an interesting observation given the substantial impact of the gain modulation on the primordial data (see C_{max} in *Figure 7*).

The addition of random noise has a profound effect on the shapes of these higher modes. This is most noticeable when comparing the bottom image pair in *Figure 7*, where the addition of noise to the synthesised data leads to the evident loss of all structure pertaining to both the underlying flaw and the emissivity artefact. This structure is still preserved within the modal representation, but is presumably swamped by noise or projected elsewhere.

A final test of the artefact-rejecting properties of the methodology was conducted on an experimental data set. *Figure 8* shows an illustration of a titanium plate containing a milled rectangular slot. Two different types of paint were applied to the reverse face, in adjacent bands orientated normal to the slot: one a regular matt-black heat radiator paint with an emissivity (ϵ) of 0.92, and the other a visibly-transparent lacquer with $\epsilon \approx 0.79$. Both paints were applied in equal film thickness to ensure minimal difference in the time response to thermal excitation. The results of peak-contrast, time-averaging, PPT and PCT methods are shown in *Figure 9*. The peak contrast and averaged images (top row) are markedly affected by the emissivity variation, whilst the ϕ_{max} and PCM images (bottom row) show only a vertical indication relating to the machined slot. Interestingly, as observed for the simulated data, the PCM image yields a noticeably higher signal to

C_{max}

ϕ_{max}

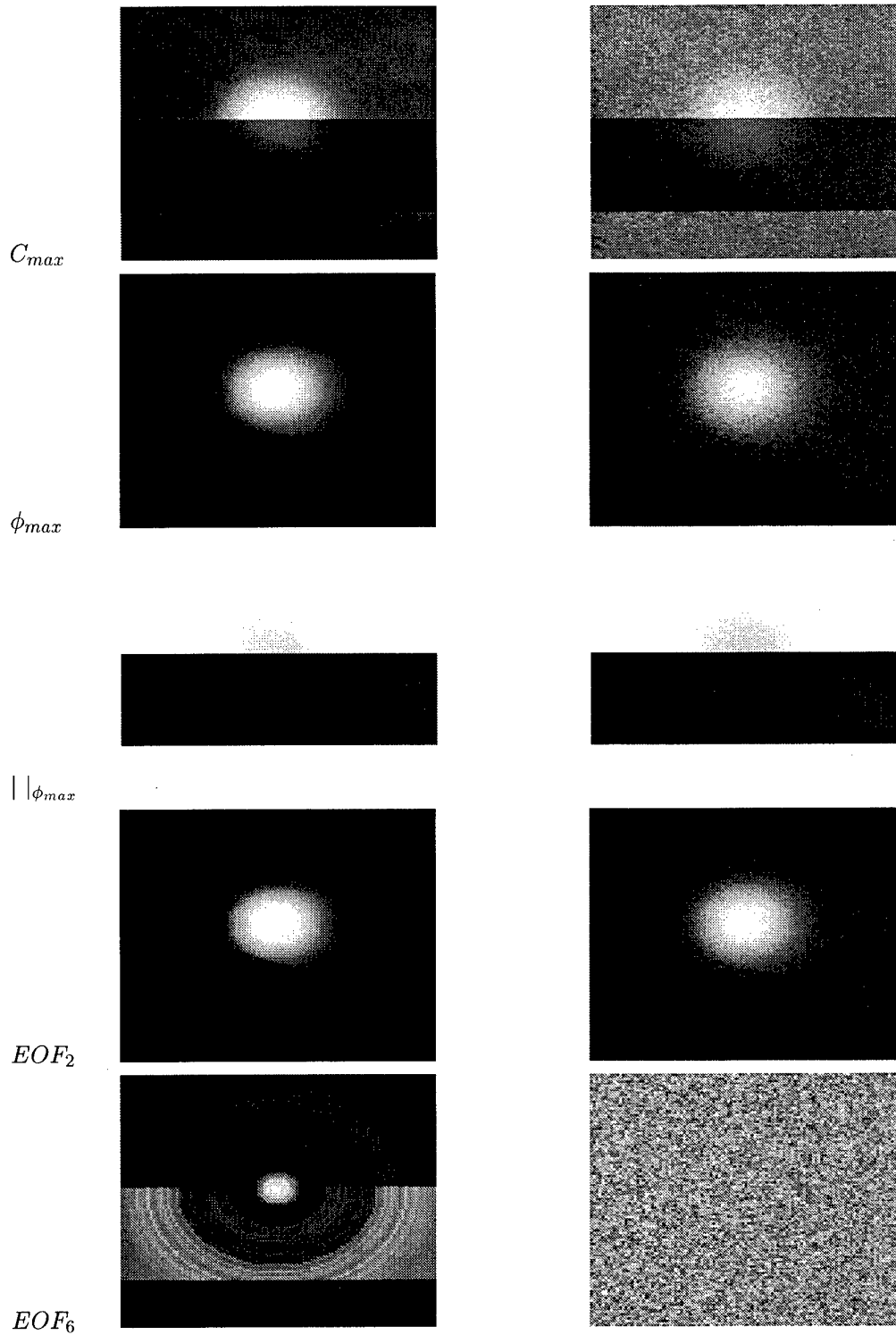$||\phi_{max}$

EOF_2

EOF_6

Figure 7: Thermograms pertaining to simulated emissivity anomaly in synthetic data (i) excluding noise (left column) and (ii) including noise (right column).
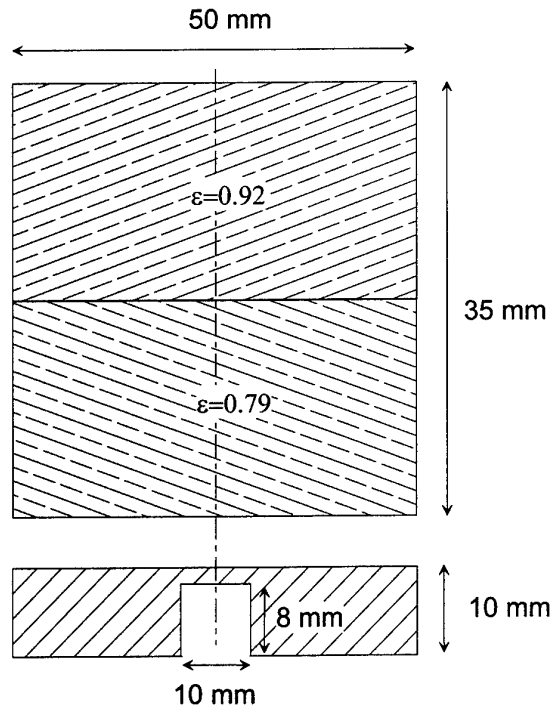
Figure 8: Details of emissivity test specimen.

noise ratio than that of the ϕ_{max} image.

3.2.1 Spatial Resolution Specimen

A final comparative assessment was performed using a spatial resolution test standard comprising an array of rectangular slots of varying width and depth milled into the back face of an aluminium panel. The relevant dimensions for the specimen are given in *Figure 10*. These notches have aspect ratios, that is the ratio of width to residual depth, varying between 1 – 11. According to an established rule of thumb, an aspect ratio of 1 defines the effective resolution threshold for active thermal inspection, so the test panel affords a good challenge for any processing methodology.

Figure 11 shows a comparison amongst phase images at multiples of the frequency resolution, the primary contrast mode and the peak contrast image. Based on casual inspection, the targets in the left column appear to be best resolved in the PCM image, followed by the peak contrast and the 4th phase image. The left target cluster was collapsed to a vertical line plot with box-car averaging applied horizontally across a window corresponding to the target width. The result is shown in *Figure 12*. These plots generally support the ranking suggested by casual inspection of the corresponding images, however whereas indications 1 and 2 appear resolved in the PCM image, the respective line plot is less conclusive. This is partly due to the presence of coherent noise, which was removed by notch-filtering to yield the bottom curve where the two narrowest targets are more readily discerned.
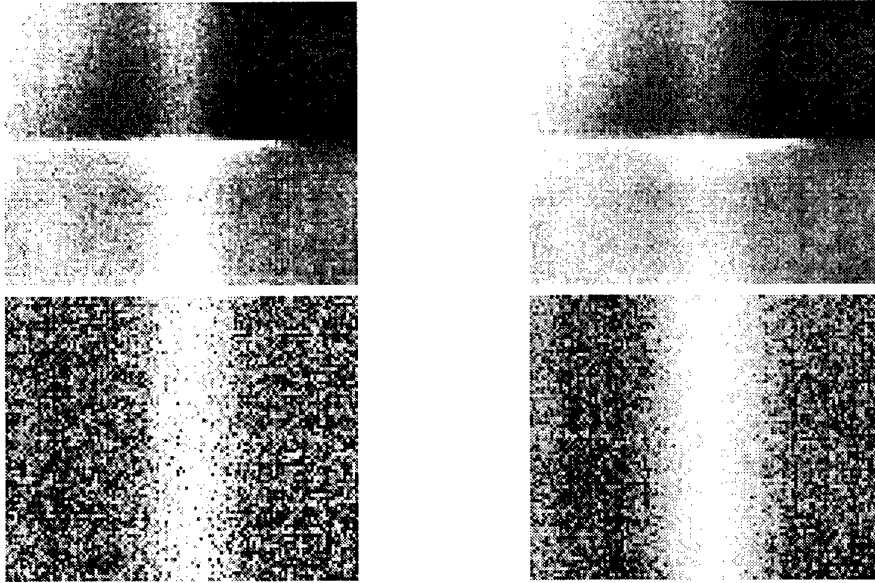
Figure 9: Emissivity test specimen thermograms. Clockwise from top left: C_{max}, $\overline{T}$, PCM, and ϕ_{max}

It is interesting to note that the phase plots show a converse trend, that is, the line plots generally furnish slightly better target indications than the corresponding images. This is brought about by the fact the noise in the phase has less spatial correlation than for the PCM, stemming from the localised nature of the phase computation, and consequently benefits more from spatial averaging. It is, however, important to understand the peculiarity of the case at hand, which allows the box-car averaging to be applied in a direction normal to the orientation of the target variation. In practice, this would seldom occur, and the application of any spatial averaging methodology, would, in general, lead to smearing and a reduction, rather than enhancement, of resolution.

The targets on the right hand side produce substantially fainter indications in the thermograms (*Figure 11*) with the line plots (*Figure 13*) furnishing a slightly better basis for flaw identification. It is noteworthy that the PCM image has an evidently higher signal to noise ratio, and, furthermore, the noise appears to be more coherent than that found in the other images, and can, accordingly, be removed without loss of detail.

4   Flaw-depth Characterisation

Discussion thus far has focused on the issue of thermal image contrast-enhancement. However, EOF analysis can also be used, in the thermal inspection context, to furnish a particularly robust and useful basis for the characterisation of flaw depth. This capability derives from a strong correlation between the time delay from excitation for the onset of a contrast and that for the first turning point in the principal component.

aluminium plate - 3mm thick
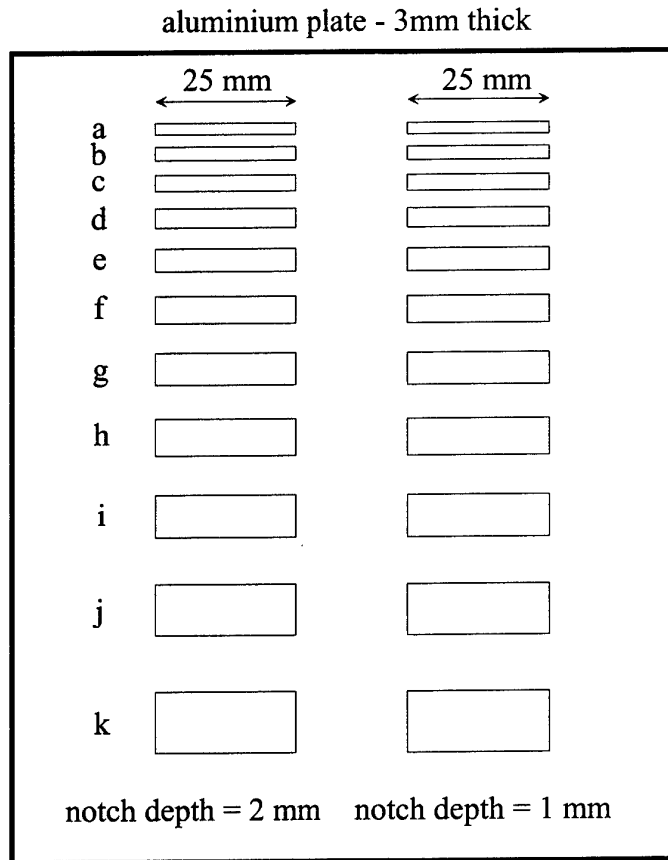
notch widths (in mm's): a=2.00, b=2.37, c=2.81, d=3.32
e=3.94, f=4.87, g=5.53, h=6.55, i=7.76, j=9.19, k=10.88

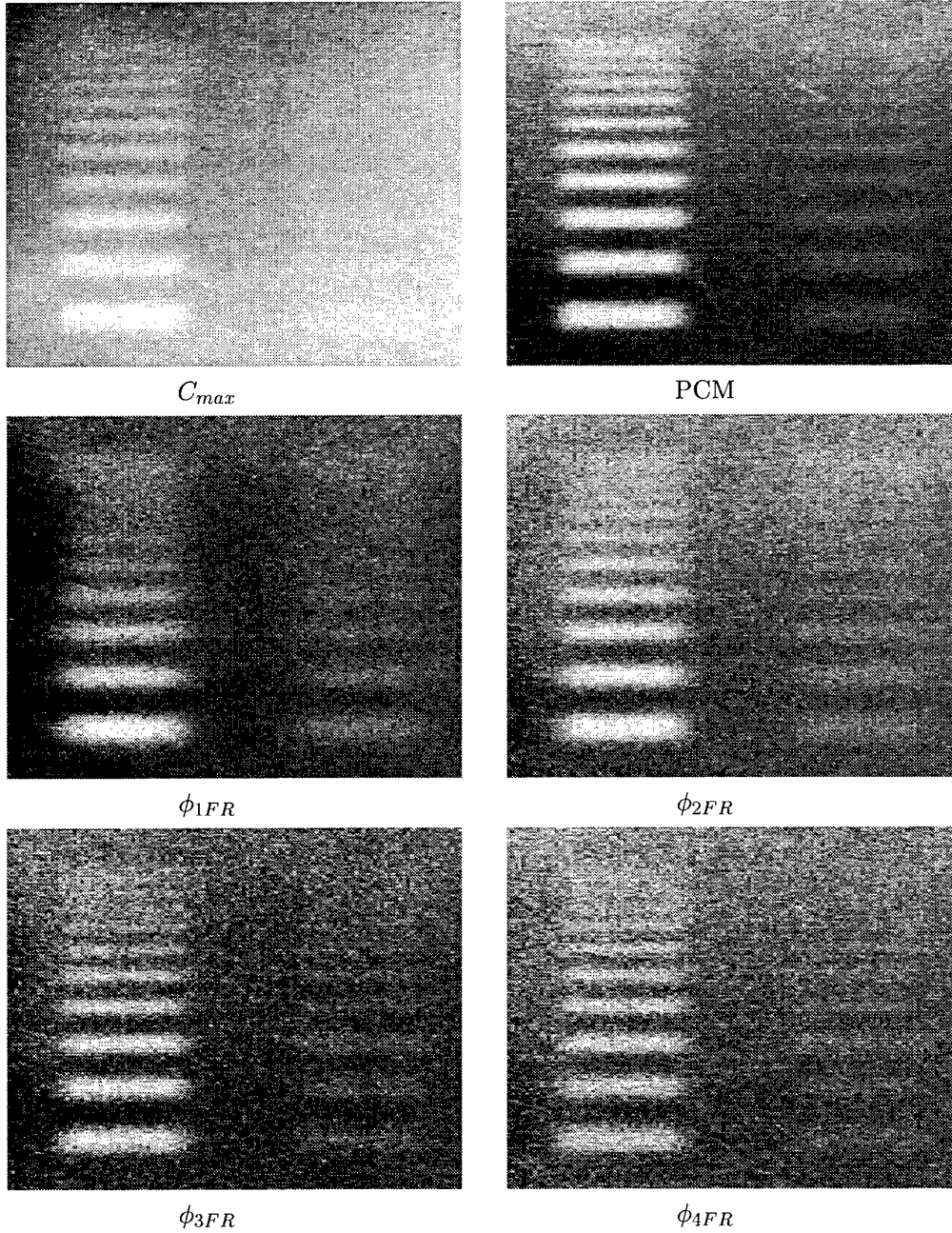*Figure 10: Schematic of spatial resolution test specimen.*
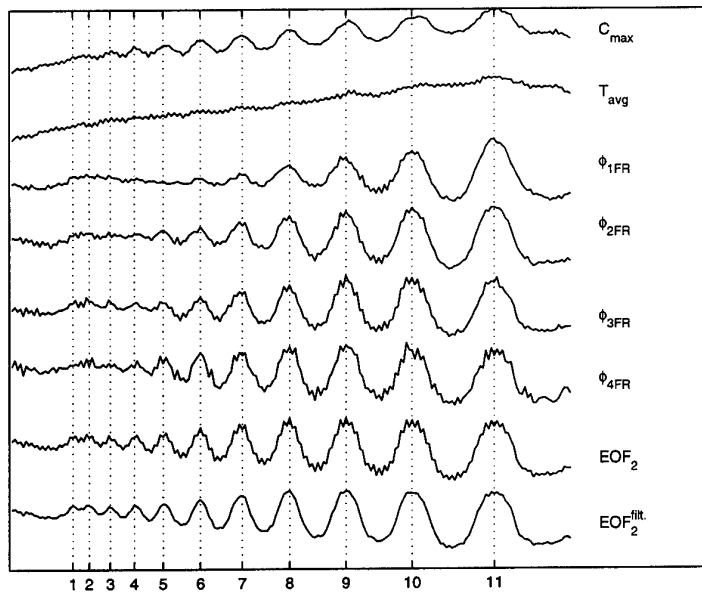
Figure 11: Processed images.

Figure 12: Line plots taken vertically through left-side defect grid.
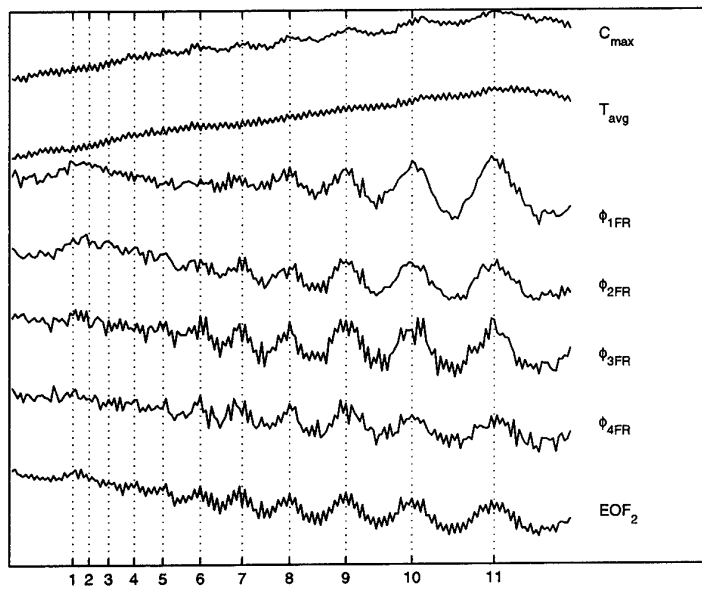

Figure 13: As for Figure 11 except through right-side defect grid.

According to classical heat-diffusion theory, a contrast begins to evolve at the moment thermal equilibrium is disturbed through, for instance, the injection of a heat pulse. In reality, a noticeable contrast indication begins to form only after a delay proportional to the square of the object depth. Various epochs in the contrast evolution can be used as a basis for characterising flaw depth. The delay to peak rate of ascent, or the inflection point, is particularly useful as it can be related through a simple analytical expression to the flaw depth, as shown by Ringermacher *et al* (1998). Specifically, given a one-dimensional slab of finite thickness L exposed to impulse heating of arbitrary strength at $x = 0$, the temperature T at the back face $x = L$ is described by the expression,

$$T(t) \propto 1 + 2 \sum_{i=1}^{\infty} -1^n \exp(-\frac{t}{t_c}n^2) \tag{9}$$

where

$$t_c = \frac{L^2}{\alpha \pi^2} \tag{10}$$

Here, α is the thermal diffusivity. The stationary point of the first time-derivative corresponds to the peak rate of ascent, viz.,

$$\sum_{i=1}^{\infty} -1^n \frac{n^4}{t_c^2} \exp(-\frac{t}{t_c}n^2) = 0 \tag{11}$$

Solving this numerically yields $t = 0.90555 t_c$. Recall that this expression pertains to a through-transmission arrangement. An extension to a single-sided configuration is trivial since the appropriate diffusion length is simply twice that for the through-thickness problem, that is $2L$. Accordingly, the inflection point occurs at

$$t_{ip} = 4 * 0.90555 t_c \tag{12}$$

It was remarked at the beginning of this section that the first turning point in the 2nd principal component furnishes a good estimate for the onset of contrast. Unlike the inflection point however, the contrast onset cannot be defined in precise analytical terms, and is consequently difficult to relate to flaw depth in a simple manner. The reason is that classical heat diffusion theory provides for an infinite speed of information propagation which, in the thermal inspection context, implies that a contrast will begin to evolve at the instant an excitation is applied.

A useful result may however be obtained by adapting the approach described by Eqns 9–11. It will be noticed that an arbitrary set of characteristic epochs, preceding the inflection point, may be derived by simply finding the stationary point of increasingly higher order time-derivatives. A heuristic study revealed that the stationary point of the third derivative furnishes a good estimate for the contrast onset, viz.,

$$\frac{\partial^4 T}{\partial t^4} = \sum_{i=1}^{\infty} -1^n \frac{n^8}{t_c^4} \exp(-\frac{t}{t_c}n^2) = 0 \tag{13}$$
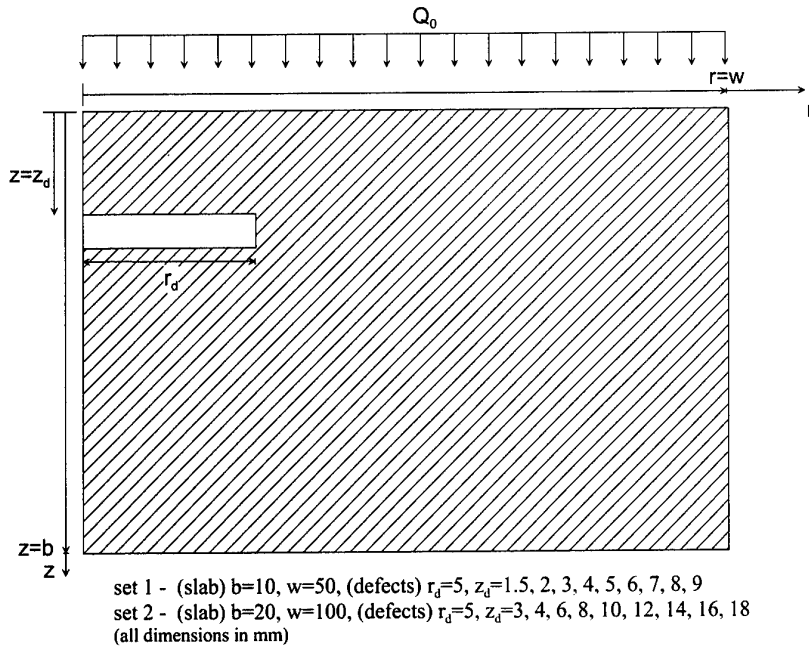
Figure 14: Cross-sectional view of axisymmetric structure considered in heat conduction simulation.

Applying the modification for a front-face inspection yields,

$$t_{co} = 1.149 t_c \qquad (14)$$

4.1 Case-Study

The inflection point and principal component approaches were applied to synthetic temperature response data furnished by a heat-conduction simulation involving an axisymmetric aluminium slab containing an air-filled void of varying depth. Simulations were run for two slab thicknesses and nine defect depths respectively, providing a total of 18 distinct cases – the relevant specimen dimensions are shown in *Figure 14*. Inflection times were computed for the surface node on the axis of symmetry ($r = 0$) by locating the peak time derivative based on a centre-difference approximation. The contrast onset time was deduced by locating the first turning point in the second principal component. These values are compared to theoretical predictions in *Figure 15*.

Focusing first on the inflection time results, it is evident that agreement between theory and numerical experiment is good for shallow flaw depths but deteriorates markedly as the depth approaches the slab thickness. In the case of a 9mm deep defect in a 10 mm slab, this amounts to an error of about 28%. The discrepancy is caused by two main factors - the assumption of a semi-infinite reference response and the omission of lateral heat flow modes in the formulation of the analytical expression. At large relative flaw depths, the contrast onset generally outperforms the inflection time, but this is mitigated by a slightly
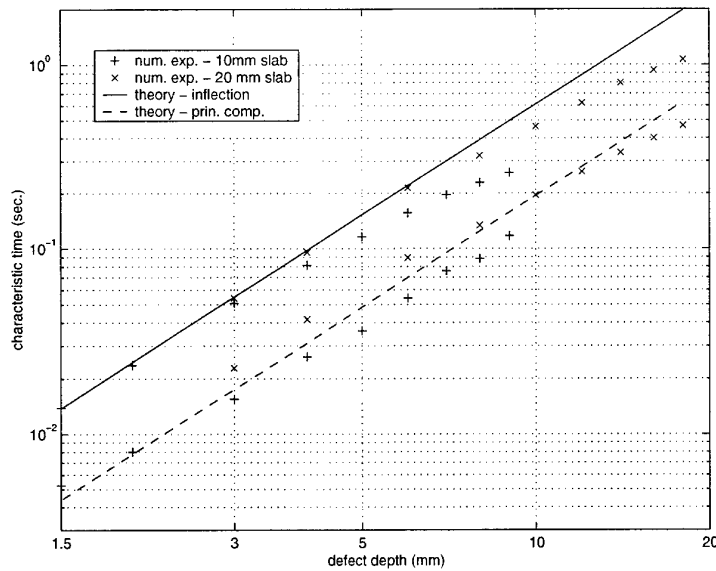
Figure 15: Comparison of characteristic times for two slab thicknesses.

inferior performance at shallow depths. On average, the contrast onset was found to be slightly more accurate.

Although no direct assessment of the relative robustness of the techniques to experimental noise was made, there is good reason to speculate that contrast onset, as predicted by the principal component, should exhibit good noise-rejection qualities. This stems from a substantial degree of data redundancy in the computation of the principal component.

A practical example is now considered. Data for this exercise was derived from a flash thermographic inspection of an Al2024 alloy slab containing a rectangular slot milled in the back face. The dimensions of the slab are 60 mm(w)×100 mm(l)×10 mm(d) whilst the slot is 10 mm wide and 6 mm deep and runs centrally down the length of the slab. The PCM and the corresponding principal component were computed from a data sequence containing 150 frames acquired at a frame rate of 540 Hz. The PCM shown in *Figure 16* clearly reveals the underlying slot. The turning point in the principal component vector (*Figure 17*) occurs 57 milliseconds after the excitation event. Based on an experimentally measured thermal diffusivity of 49 mm^2sec^{-1}, Eqn 14 yields a residual thickness estimate of 4.9 mm, which differs from the known thickness by 0.9 mm. A separate analysis of the contrast evolution confirmed good synchronicity between the contrast offset and the turning point in the principal component, leaving, as possible alternative sources of error, a biased thermal diffusivity value or deficiencies in the formulation of Eqn 14.

4.2 General Comments

The methodology is only in a preliminary stage of development, with a more complete assessment needed to better understand its capabilities and limitations relative to conventional approaches. Some shortfalls and advantages are clearly evident based on the limited
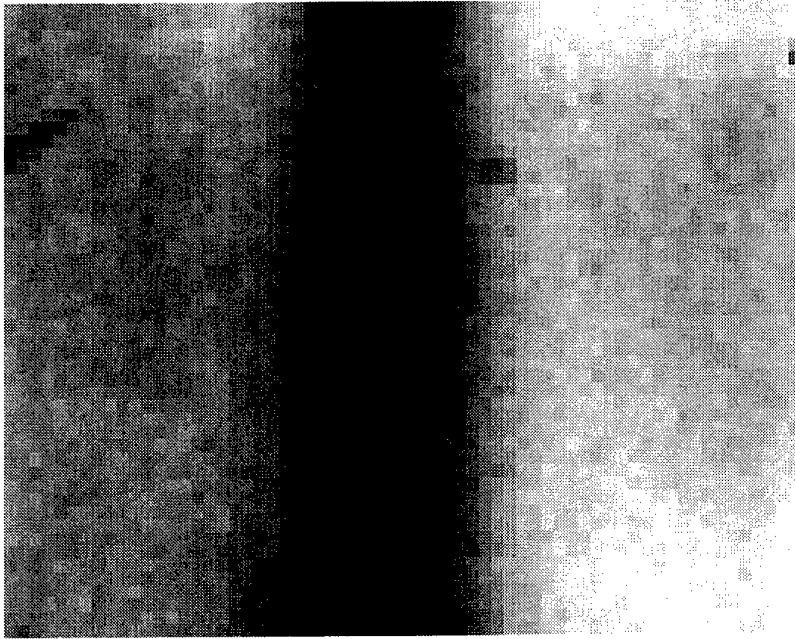
Figure 16: PCM for an Aluminium Al2024 slab with a rectangular slot.
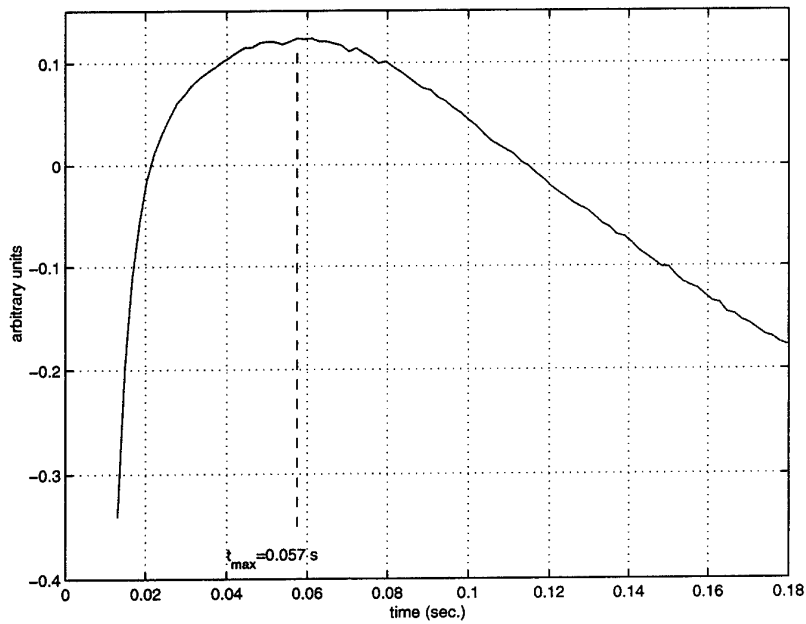

Figure 17: Principal component for the PCM shown in Figure 16.

analysis conducted in the present study, and it is worthwhile providing a brief outline of these.

One of the salient advantages, as stated earlier, is that it does not rely on the explicit formation of a contrast evolution and therefore eliminates the need for identifying a reference response. Methods reliant on the inflection time are also particularly susceptible to noise because of the need to differentiate the contrast response evolution. With this in mind, there is reason to expect that the proposed method should furnish higher levels of robustness because no differentiation is involved and the principal component vector is computed from the time evolution of a large number of data points providing a high level of redundancy. Other methods are available that are also not reliant on the formation of a contrast response, for instance that reported in Shepard *et al* (2001), where flaw depth is characterised on the basis of the time of departure of an observed response from ideal behaviour. The robust estimation of the departure point is not trivial and generally benefits from a parameterisation of the observations, which is not required by the proposed methodology.

An obvious practical limitation is that the method renders a regional rather than point-wise estimate of flaw depth. Consequently, the method, in its current form, cannot furnish estimates of the distribution of flaw depth within a flawed zone, but rather provides an estimate of the average depth. It is important to understand that since most point-wise analysis techniques do not accommodate lateral heat diffusion modes, they too furnish a spatially-averaged estimate of depth, but clearly not in the intrinsic manner of the proposed methodology. Future efforts should consider the potential for computing flaw-depth distributions by means of a segmented decomposition where sections of an image (whether lines or blocks) are decomposed independently and the results then recombined.

Another general disadvantage of the technique is the high computational expense of singular value decomposition, compared to phase or time-derivate computation. The standardised data matrix formed by collapsing a thermal data "cube" is invariably large for most practical inspection problems and computationally expensive to decompose, despite the implementation of efficient numerical strategies. For instance, on a 1.7 GHz processor, decomposition of a sequence of 200 frames, each with a square 128 pixel array, takes approximately 15 seconds, compared to 2.5 seconds for the calculation of a phase map.

Although not explored in the present study, the potential for achieving substantial compression of thermographic data sequences through mode-based low-pass filtering is obvious. Subsequent data reconstruction, based on only the first few empirical orthogonal functions would presumably produce a much cleaner variant of the original data sequence.

5 CONCLUSION

A method has been described that provides an integrated framework for the enhancement of flaw contrast and the characterisation of flaw depth. Analyses have shown that the levels of contrast enhancement are comparable to if not better than those furnished by pulse phase thermography. The proposed methodology also offers the practical advantage of not requiring the user to determine a priori the frequency at which maximum phase

contrast occurs, and is, accordingly, simpler to implement. A single computational process yields both an image containing spatial contrasts relating to underlying structural flaws, and a characteristic time evolution that provides a robust and simple basis for the estimation of flaw depth. The process is numerically intensive and generally requires more computational effort than point-wise processing techniques, but this is mitigated by its provision of a more complete description of underlying flaws. The method has a wide scope of application and is not restricted to the material loss problems considered in the present study. Supplementary work has shown the technique to be equally effective on composite degradation problems.

References

. Couturier, J. P., Maldague, X. A., (1997), "Pulse Phase Thermography of Aluminum Specimens",*Proceedings of SPIE – Thermosense XIX*, **3056**, pp. 170–175.

. Cramer, K. E., Howell, P. A., and Syed, H. I., (1995), "Quantitative Thermal Imaging of Aircraft Structures",*Proceedings of SPIE - Thermosense XVII*, **2473**, p. 226.

. Emery, W. J., and Thomson, R. E., (1998). *Data Analysis Methods in Physical Oceanography*, Elsevier, New York.

. Maldague, X., and Marinetti, S., (1996), "Pulse Phase Infrared Thermography",*J. Appl. Phys.*, **79**, pp. 2694-2698.

. Marinetti, S., Plotnikov, Y. A., Winfree, W. P., and Braggiotti, A., (1999), "Pulse Phase Thermography for Defect Detection and Visualization ",*Proceedings of SPIE – NDE of Aging Aircraft, Airports and Aerospace Hardware*, **3578**.

. Plotnikov, Y. A., Rajic, N., and Winfree, W. P., (2000), "Means of Eliminating Background Effects for Defect Detection and Visualisation in Infrared Thermography",*Optical Engineering*, **39**, pp. 879-884.

. Rajic, N., (2000), "A Quantitative Approach to Active Thermographic Inspection for Material Loss Evaluation in Metallic Structures", *Journal of Research in Nondestructive Evaluation*, **12**, pp. 119-131.

. Rajic, N., (2001), "Noise in Infrared Thermography - in Infrared and Thermal Testing, Nondestructive Testing Handbook Vol. 3", Maldague, X. P. V & Moore, P. O., eds., American Society for Nondestructive Testing, pp. 111-118.

. Ringermacher, H. I., Mayton, D. J., Howard, D. R., and Cassenti, B. N., (1998), "Towards a Flat-Bottom Hole Standard for Thermal Imaging". *Review of Progress in Quantitative Nondestructive Evaluation*, bf 17, Eds: D. O. Thompson and D. E. Chimenti, Plenum Press, New York.

. Shepard, S. M., Lhota, J. R., Ahmed, T., Rubadeaux, B. A., and Wang, D., (2001), "Quantification and Automation of Pulse Thermographic NDE". *Nondestructive Evaluation of Materials and Composites V, Proceedings of SPIE*, bf 4336, Eds: G. Y. Baaklini, E. S. Boltz, S. M. Shepard, and P. J. Shull.

. Winfree, W. P., (1998), "Enhanced Thermographic Detection of Delaminations with Computational Pulse Shaping", Review of Progress in QNDE, Proceedings of the Twenty-Fourth Symposium held in San Diego, California, July 27 - August 1, 1997, Edited by Donald O. Thompson and Dale E. Chimenti, Iowa State University, Ames, Plenum Press, Vol 17A, pp. 441–448.

. Winfree, W. P., and Heath, D. M., (1998), "Thermal Diffusivity Imaging of Aerospace Materials and Structures", in Thermosense XX, edited by J. R. Snell and R. N. Wurzback, SPIE Proceedings Series Vol. 3361, Bellingham WA, pp. 282–290.

DISTRIBUTION LIST

Principal Component Thermography
N. Rajic

Number of Copies

DEFENCE ORGANISATION

S&T Program

Chief Defence Scientist	
FAS Science Policy	
AS Science Corporate Management	1
Director General Science Policy Development	
Counsellor, Defence Science, London	Doc Data Sht
Counsellor, Defence Science, Washington	Doc Data Sht
Scientific Adviser to MRDC, Thailand	Doc Data Sht
Scientic Adviser Joint	1
Navy Scientific Adviser	Doc Data Sht
Scientific Adviser, Army	Doc Data Sht
Air Force Scientific Adviser	1
Director Trials	1

Aeronautical and Maritime Research Laboratory

Director, Aeronautical and Maritime Research Laboratory	1
Chief, Airframes and Engines Division	1
RLACS	1
Nik Rajic	5
Steve Lamb	1
Steve Galea	1
David Rowlands	1

DSTO Library and Archives

Library Fishermens Bend	1
Library Edinburgh	1
Australian Archives	1
Library, MOD, Pyrmont	Doc Data Sht
Library, MOD, HMAS Stirling	Doc Data Sht
US Defense Technical Information Center	2
UK Defense Research Information Center	2
Canada Defence Scientific Information Service	1
NZ Defence Information Centre	1

National Library of Australia	1

Capability Systems Staff

Director General Aerospace Development	1

Knowledge Staff

Director General Command, Control, Communications and Computers (DGC4)	Doc Data Sht

Army

ABCA National Standardisation Office, Puckapunyal	4
SO (Science), Deployable Joint Force Headquarters (DJFHQ)(L), Enoggera QLD	Doc Data Sht

Air Force

DGTA- DAIRENG	1
DGTA- DAIRMAINT	1
OIC - NDTSL	1
NDT Officer NDTSL	1

Intelligence Program

DGSTA Defence Intelligence Organisation	1
Manager, Information Centre, Defence Intelligence Organisation	1

Corporate Support Program

Library Manager, DLS-Canberra	1
MS Sam Doran, Defence Library Service - Syndey West	1

UNIVERSITIES AND COLLEGES

Australian Defence Force Academy Library	1
Head of Aerospace and Mechanical Engineering, ADFA	1
Serials Section (M List), Deakin University Library, Geelong, VIC	1
Hargrave Library, Monash University	Doc Data Sht
Librarian, Flinders University	1

OTHER ORGANISATIONS

NASA (Canberra)	1
AusInfo	1

OUTSIDE AUSTRALIA

Elliot C. Cramer, Mail Stop 231, NASA Langley Research Center, Hampton, VA 23681-0001, USA	1

William R. Davis, Naval Air Systems Command, Research & Engineering Group, 48066 Shaw Rd, Patuxent River, MD 20670-5304, USA	1
Ignacio Perez, Office of Naval Research, Code 332, 800 N Quincy Street, Arlington, VA 22217, USA	1
Yuri A. Plotnikov, GE Corporate Research & Development, Building KW, One Research Circle, Niskayuna, NY 12309, USA	1
Harry I. Ringermacher, GE Corporate Research & Development, Building KW, One Research Circle, Niskayuna, NY 12309, USA	1
Steven M. Shepard, Thermal Wave Imaging, 845 Livernois, Ferndale, MI 48220, USA	1
William P. Winfree, Mail Stop 231, NASA Langley Research Center, Hampton, VA 23681-0001, USA	1
Joseph N. Zalameda, Mail Stop 231, NESB, NASA Langley Research Center, Hampton, VA 23681-0001, USA	1

ABSTRACTING AND INFORMATION ORGANISATIONS

Library, Chemical Abstracts Reference Service	1
Engineering Societies Library, US	1
Materials Information, Cambridge Science Abstracts, US	1
Documents Librarian, The Center for Research Libraries, US	1

INFORMATION EXCHANGE AGREEMENT PARTNERS

Acquisitions Unit, Science Reference and Information Service, UK	1
Library – Exchange Desk, National Institute of Standards and Technology, US	1
National Aerospace Laboratory, Japan	1
National Aerospace Laboratory, Netherlands	1

SPARES

Library Edinburgh	5

Total number of copies:	**65**

DEFENCE SCIENCE AND TECHNOLOGY ORGANISATION DOCUMENT CONTROL DATA	1. CAVEAT/PRIVACY MARKING

2. TITLE Principal Component Thermography	3. SECURITY CLASSIFICATION Document (U) Title (U) Abstract (U)

4. AUTHOR N. Rajic	5. CORPORATE AUTHOR Aeronautical and Maritime Research Laboratory 506 Lorimer St, Fishermans Bend, Victoria, Australia 3207

6a. DSTO NUMBER DSTO–TR–1298	6b. AR NUMBER 012-294	6c. TYPE OF REPORT Technical Report	7. DOCUMENT DATE April 2002

8. FILE NUMBER M1/9/1061	9. TASK NUMBER DST 01/122	10. SPONSOR DGTA	11. No OF PAGES 23	12. No OF REFS 12

13. URL OF ELECTRONIC VERSION http://www.dsto.defence.gov.au/corporate/ reports/DSTO–TR–1298.pdf	14. RELEASE AUTHORITY Chief, Airframes And Engines Division

15. SECONDARY RELEASE STATEMENT OF THIS DOCUMENT

Approved For Public Release

OVERSEAS ENQUIRIES OUTSIDE STATED LIMITATIONS SHOULD BE REFERRED THROUGH DOCUMENT EXCHANGE, PO BOX 1500, SALISBURY, SOUTH AUSTRALIA 5108

16. DELIBERATE ANNOUNCEMENT

No Limitations

17. CITATION IN OTHER DOCUMENTS

No Limitations

18. DEFTEST DESCRIPTORS

Thermography F/A-18 aircraft Structural design Nondestructive tests	Military aircraft F-111 aircraft Aircraft structures

19. ABSTRACT

This report describes a robust computational framework for the qualitative enhancement and quantitative interpretation of active thermographic inspection data. Singular Value Decomposition is used to reduce an appropriately constructed matrix of raw pixel values to a set of orthogonal functions that compactly describe the key spatial and temporal variations relating to underlying structural anomalies. Tests against synthetic and experimental data are described that underscore the practical efficacy of the methodology, and demonstrate significant advantages compared to more traditional methods of processing.

DEFENCE
SCIENCE & TECHNOLOGY